JTTEE5 19:575–585
DOI: 10.1007/s11666-009-9455-6
1059-9630/$19.00 © ASM International

The Effects of Successive Impacts and Cold Welds on the Deposition Onset of Cold Spray Coatings

Yuming Xiong, Gyuyeol Bae, Xiang Xiong, and Changhee Lee

(Submitted May 5, 2009; in revised form September 7, 2009)

In this study, the impact and deposition behavior of nickel particles onto relatively soft 6061-T6 aluminum alloy and copper substrates in a kinetic spray process was investigated by comparing individual particle impact with full coating deposition. The results indicated that the deposition onset of nickel coatings on the two substrates follows different deposition mechanisms depending on corresponding deformability of the impact couples (substrate and particle). Nickel particles were hardly attached onto the relatively soft 6061-T6 substrate in case of individual impact, but the deposition onset of full coating took place depending on embedding, tamping of successive impact and metallurgical "cold welds" of viscous metal at impact interface when the impinging particles' velocity was relatively low. In case of Ni-Cu impact, the bonding formed at the peripheral impact interface dominated the deposition onset of nickel coating due to the comparable deformability of the impact couples (Ni and Cu).

Keywords cold spray coating onset, cold welds, rebound, successive impact, transmission electron microscopy

1. Introduction

The cold gas dynamic spraying process (also known as "cold spray" or "kinetic spray") is a newly emergent technology designed to deposit coatings onto substrate through a high speed (300-2000 m/s) impact and plastic deformation of micron-sized particles (typically 5-50 μm) at a high-strain rate (~10^9/s) (Ref 1, 2). This process is considered a solid-state process as the impact temperature of the involved materials (particle and substrate) never reaches their melting points during deposition. As a result, both the properties and microstructure of the initial feedstock can be preserved in the final coatings. Accordingly, it is attractive for the low-temperature process to deposit oxygen- or/and thermo-sensitive and nanostructural coatings since external heat may not be inputted.

Although the cold spray has been employed to fabricate metals (Ref 3, 4), alloys (Ref 5, 6), nanostructural (Ref 6-8), composites (Ref 9, 10), metallic glasses (Ref 11), even ceramic (Ref 12), and cermet (Ref 13-15) coatings, the deposition or bonding mechanisms of the coatings have not been precisely determined. It has been confirmed that each impact system in the cold spray process typically has its own critical velocity v_{cr} above which coating occurs and the modeled adiabatic shear instability (ASI) begins to form at the particle-substrate interface (Ref 2). Depending on the location, the thermal softening dominant over strain hardening is possible with a locally shear instability which is linked with the abnormal temperature/strain rise and stress collapse at the impact interface. The viscous-alike materials within the thermal softening region is compressed and pushed out quickly toward the periphery of the particle to form a jet. It also has been proposed that the violent action of the jets break down the native oxide films on the particle to enable the intimate contact and form metallurgical bonds across the two lattices (Ref 16). Accordingly, ASI as one of the deposition mechanisms of cold spray coatings has been used as a criterion to evaluate critical velocity of many impact systems in the cold spray process (Ref 2). That is, the occurrence of ASI at the impact interface suggests the transient from erosion of substrate to deposition of particle.

Meanwhile, Wu et al. have proposed another understanding to the deposition onset of cold spray coatings by considering the conversion of kinetic energy to adhesion energy of impinging particles (Ref 17). Even though the ASI induced locally thermal softening exists at the impact interface, the elastic recovery (rebound) of incident particle is inevitable during the elastic unloading following the elastic-plastic loading in the cold spray process. Only in the case that adhesion energy surpasses rebound energy, the impinging particle can be captured, and the coating can be triggered. The experimental bond ratio (BR) of Al-Si powder on mild steel as a function of particle impinging velocity in a kinetic spray process has been

Yuming Xiong and **Xiang Xiong**, State Key Laboratory for Powder Metallurgy, Institute of Powder Metallurgy Research in Central South University, Changsha 410083, China; and **Gyuyeol Bae** and **Changhee Lee**, Kinetic Spray Coatings Laboratory (NRL), Division of Materials Science and Engineering, Hanyang University, 17 Haengdang-Dong, Seongdong-Gu, Seoul 133-791, Korea. Contact e-mails: ymxiong@hotmail.com and chlee@hanyang.ac.kr.

in a good agreement with this theory (Ref 17). Recently, the rebound and detaching of the impinged particles from the substrate has been confirmed by the observation of high-resolution electron microscopy at the impact interface (Ref 18).

In this paper, the individual impact and full coating deposition of nickel onto relatively soft 6061-T6 aluminum alloy and copper substrates have been performed. The deposition process of coatings and the microstructural evolution at the bonding interface have been investigated by scanning/transmission electron microscopy (SEM/TEM) observation. The influences of subsequent impact and cold welds of the thermally softened metals on the deposition onset of kinetic sprayed coatings on both substrates have been discussed.

2. Experimental

A commercially available CGT kinetic spraying system (KINETIKS 3000, Germany) was used in the research. A de-Laval type converging-diverging MOC nozzle with round exit was used. The diameter of nozzle exit and the diameter ratio of exit to throat are 6.34 mm and 2.34, respectively. Nitrogen or helium gas was used as the process gases. The impact velocity of nickel particles varied through changing type (nitrogen and helium), temperature (300- 550 °C) and pressure (15-29 bar) of process gas. The carrier gas was set as 7% of process gas. Two deposition modes were used as follows: low powder feed (6 g/min) with high nozzle traveling speed (600 mm/s) for individual particle impact, and high powder feed (24 g/min) with low nozzle traveling speed (100 mm/s) for full coating deposition.

The polished 6061-T6 aluminum alloy and copper sheets were used as substrates, which were fixed at 30 mm in front of the nozzle exit. The Vickers hardness of the substrates was measured by a Microhardness tester (HMV-2, Shimadzu) using a load of 1.961 N for 10 s. The hardness for each sample was averaged over ten readings.

A commercial, pure nickel powder (Metco 56F-NS) was used as feedstock. The particle size distribution was analyzed by a particle size analyzer (Mastersizer S, Malvern). As shown in Fig. 1(a), a nickel powder with a mean size of 35 μm was nearly spherical. D_{10}, D_{50}, D_{90} of the powder are 27, 40, and 60 μm, respectively. The distribution in feedstock particle size is given in Fig. 1(b). The hardness and elastic modulus of nickel particles were measured by nanoindentation technique (Nanoindenter XP, MTS) with a diamond Berkovich (three-sided pyramid) indenter mounted in a nanoindenter at a constant strain rate (0.05 s^{-1}). The physical properties of nickel feedstock and the two substrates are given in Table 1 (Ref 19).

In the case of individual particle impacts, the surface and cross-sectional micrographs of the craters and deposits were characterized by SEM (JSM 5600, JEOL). The BR, defined as the fraction of bonded particles (deposits) to the total incident particles (craters plus deposits), was calculated by an image analysis method,

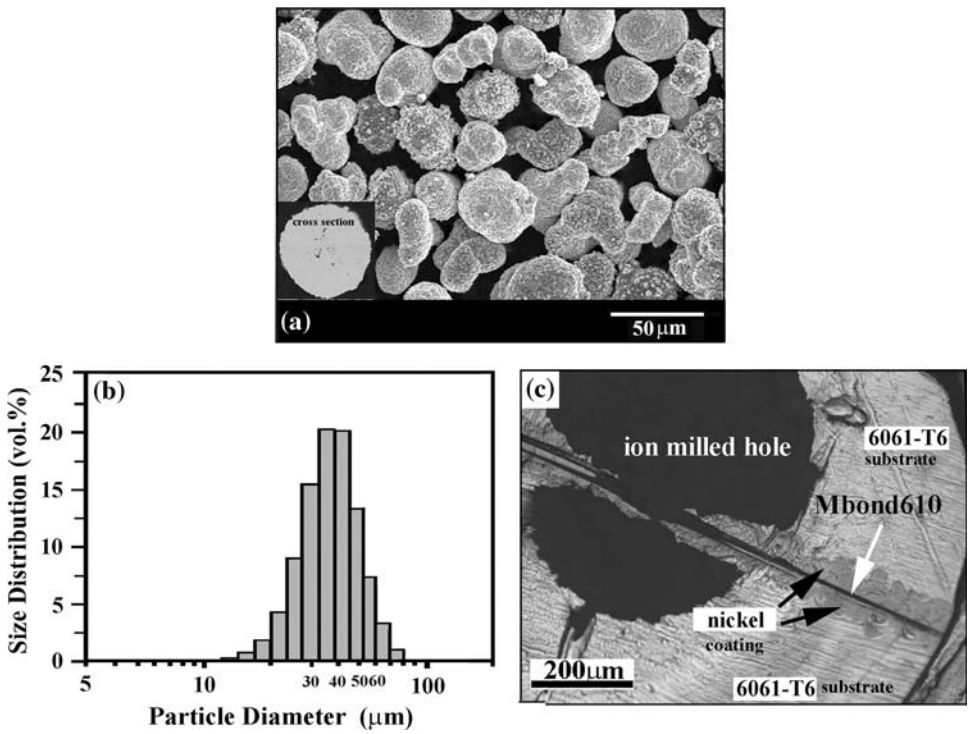

Fig. 1 The morphology (a) and size distribution (b) of the initial nickel feedstock powder

Table 1 Physical properties of Ni feedstock and 6061-T6 and copper substrate (Ref 19)

	Hardness, GPa	Melting point, °C	Elastic modulus, GPa	Shear modulus, GPa	Specific heat, J kg^{-1} K^{-1}
Nickel	5.84	1452	209.4	76	476
6061-T6	1.2	660	69	26	877
Copper	0.97	1083	124	46	383

and compared with the deposition efficiency (DE) of the corresponding full coating deposition case in which one pass spraying was used to describe the deposition onset of nickel coating on the substrates. DE was defined as the mass gain of specimens divided by the consumption of spray powder which depends on the spraying time and powder feed rate.

To prepare the TEM samples, a thicker nickel coating was deposited on 6061-T6 substrate by two passes spraying with a powder feed rate of 24 g/min using 400 °C-25 bar helium process gas. In this case, it is possible to easily find a ''tri-phase'' boundary (such as interfaces among two particles and the substrate) by increasing the possibility of successive impacts to figure out the effect of subsequent impacts on the bonding of impinging particles. Two polished nickel coating surfaces were bonded face to face with an opaque epoxy of MBond 610 followed by a solidification process at 120 °C for 2 h in air. The specimens were sliced into pieces with a thickness of 1.5 mm. The cross-sectional specimens were polished and mounted on a copper grid with a diameter of 3 mm and a central aperture of 800 μm in diameter. The aperture should be free from epoxy and the bonded interface of the two coatings was centered. The sample was polished down to a thickness of 100 μm, dimpled, and ion milled for FE-TEM observation at excitation voltages of 200 kV. The cross-sectional TEM sample for interfacial microstructure examination is shown in Fig. 1(c).

To explain the experimental results, the impacts of an individual nickel particle onto Cu substrates and of successively double nickel particles with the same particle velocity of 600 m/s onto 6061-T6 aluminum alloy were simulated through finite elements analysis (FEA) using a commercial software ABAQUS/Explicit (Version 6.7-2) (Ref 20). The initial configuration, boundary conditions, meshing methods, and detailed simulation information were given in Ref 21.

3. Results

3.1 Individual Particle Impact

As given in Table 2, no nickel particles could be bonded on either of the substrates when sprayed at the parameters of 550 °C-29 bar nitrogen gas in the case of individual particle impact. The BR values close to zero explain well the concept of critical velocity. This is because the velocity of nickel particle delivered by 550 °C-29 bar nitrogen gas was less than the critical velocity of nickel particle on either of the substrates.

Table 2 Bonds ratio (BR) of individual Ni particle impacts and DE of full area coatings on the two substrates with respect to the spray conditions

	On 6061-T6		On copper	
	BR, %	DE, %	BR, %	DE, %
550 °C-29 bar-N_2	<1	25.4	<1	4.7
400 °C-25 bar-He	22.5	43.7	53.6	45.4

The BR of nickel on both substrates increases with particle velocity by changing the process gas from nitrogen to helium. A discrepancy in BR related to the nature of the substrate becomes observable. In case of 400 °C-25 bar helium process gas, the BR of nickel on the relatively soft aluminum alloy (22.5%) is much lower than that on copper (53.6%). The speed of impinging particles was high enough (above critical velocity) to deform particle and substrate comparably and get deposits on copper substrate. Nevertheless, the high speed nickel particle like a rigid ''bullet'' penetrated the relatively soft 6061-T6 substrate. Because of the high rebound force and lack of the tamping of successive impacts, it seems difficult to maintain the attachments of nickel in the crater in the 6061-T6 substrate. Figure 2 shows the different deposition behavior of nickel particle on both substrate, and the deep crates are visible in 6061-T6 substrate after impact.

As shown in Fig. 3, the BR of nickel particle on both substrates shows an interesting tendency with the velocity of particles sprayed using helium. On the relatively soft aluminum alloy, the BR decreases with increasing particle velocity which is calculated using an empirical equation proposed in Ref 22, but an inverse tendency can be observed on copper substrate. Also, an optimum particle velocity for a peak value of BR on Cu substrate can be obtained. The discrepancy of BR indicates different deposition mechanisms of nickel particles on the two substrates and will be discussed in detail in following sections.

As shown in Fig. 4, the morphologies of craters and deposits also suggest different impact behaviors of nickel particle on both substrates. The slightly deformed nickel particle penetrated deeply below the aluminum alloy surface, and there was considerable deformation of the originally flat substrate surface. The crater in the aluminum alloy is cylindrical in shape. In the substrate of copper, however the crater is semi-ellipsoidal in shape. The deformed nickel particle in an ellipsoidal shape is buried below the copper surface. The crater fringes tend to pack the nickel deposit. Also, one can find that an intimate

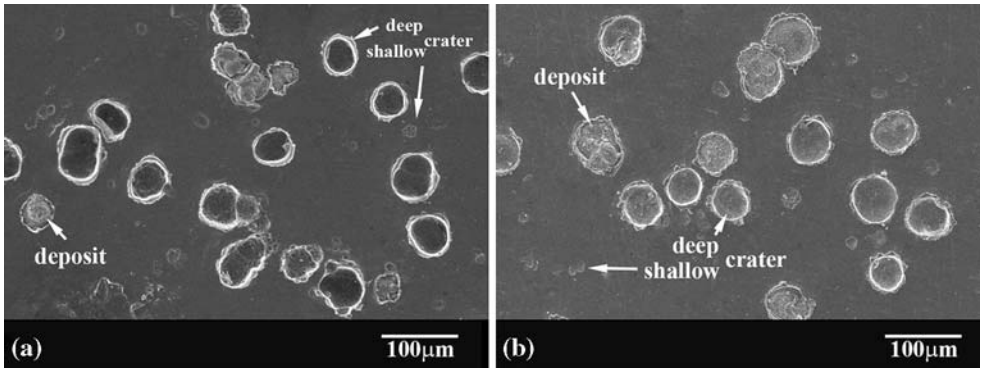

Fig. 2 Surface morphologies of 6061-T6 (a) and Cu (b) substrates after individual particle impact of Ni powder delivered by 400 °C-25 bar helium gas

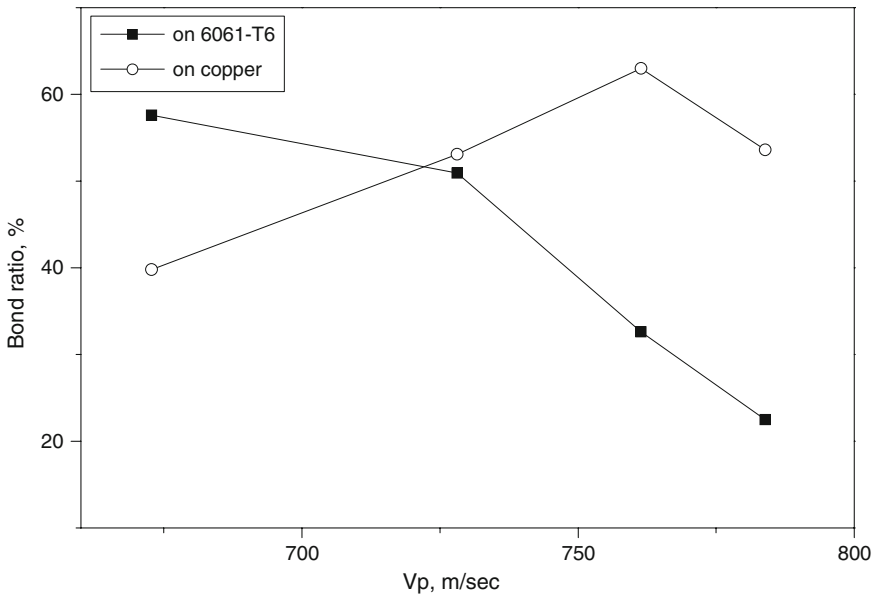

Fig. 3 The BRs of individual Ni particle impacts on 6061-T6 and Cu substrates as a function of particle velocity

contact of nickel with copper happens within the shear region (marked as E and E' in Fig. 4b and d), and a seam forms within the normal strain region (marked as C in Fig. 4b and d). In both cases, nickel does not participate in jetting because of its insufficient deformation and low impact temperature upon impact.

3.2 Full Coating Deposition

Interestingly, the deposition behavior of nickel powder in case of full coating deposition seems different from the correspondingly individual impact case. Although nickel coating could hardly be obtained on copper (DE = 4.7%) in case of nitrogen gas (e.g. 550 °C-29 bar), the DE of 25.4% was measured on the relatively soft aluminum alloy. In case of 400 °C-25 bar helium, the DEs of full coating on both substrates are comparable (43.7% on aluminum and 45.4% on copper) although there is a discrepancy in BR at the same parameter in case of individual particle impact as mentioned above. It indicates that the tamping of successive impacts enhances the deposition onset of cold spray coatings on the relatively softer substrate (i.e., 6061-T6 in this study).

As shown in Fig. 5(a) and (b), it is found that a thin nickel coating can be successfully deposited on the 6061-T6 substrate but almost no coating on copper in case of full coating deposition using 550 °C-29 bar nitrogen gas. It is interesting that a thin nickel film even can be achieved on 6061-T6 alloy substrate using lower parameters, such as 300 °C-15 bar nitrogen gas. However, although it is easier for the deposition onset of nickel coating on a softer substrate, the growth of nickel coating on the previously deposited nickel layer relies on a particle velocity which must exceed the critical velocity of nickel to nickel impact system.

In case of spraying using 400 °C-25 bar helium, the nickel coating can form on the both substrates as shown in Fig. 5(c) and (d) indicating particle velocity is over the

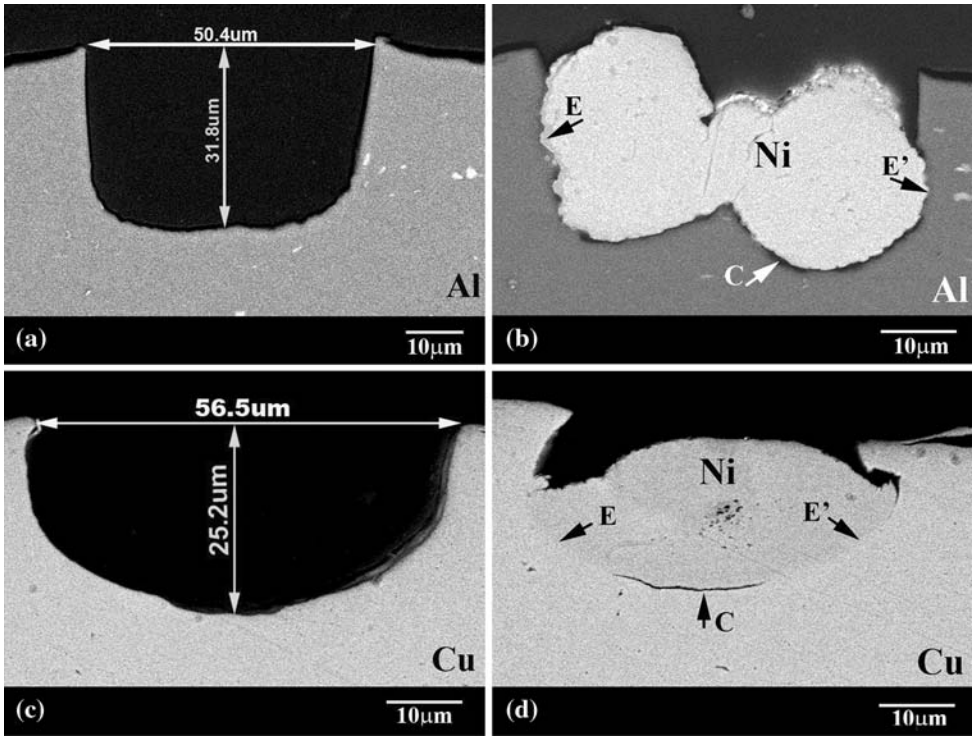

Fig. 4 The morphologies of craters and deposits on 6061-T6 and Cu substrates by individual particle impacts using 400 °C-25 bar helium process gas

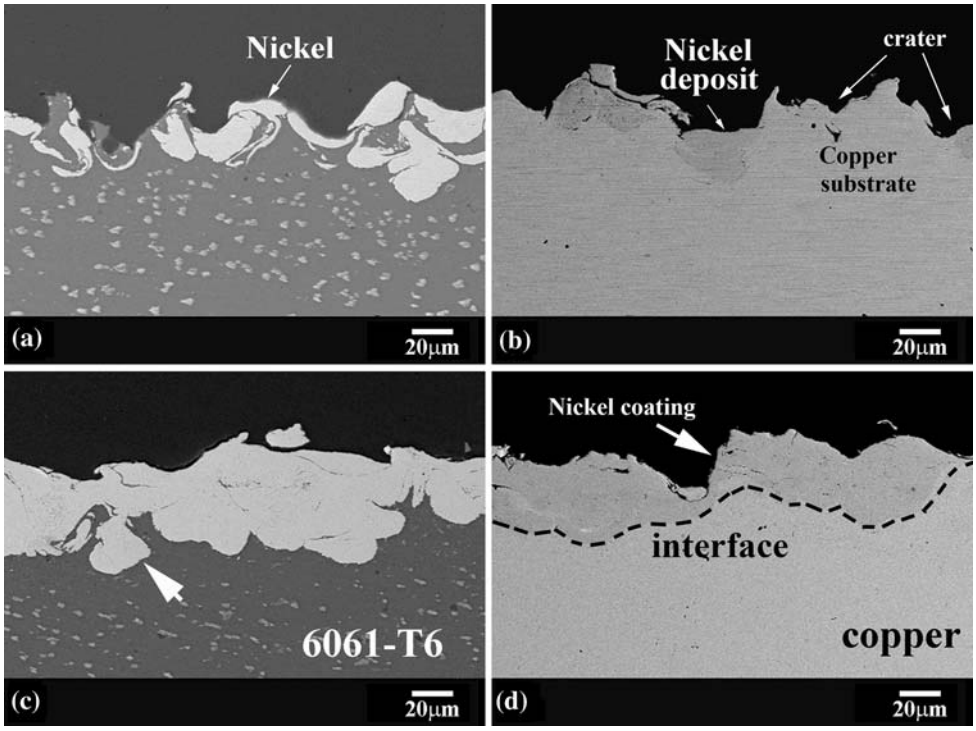

Fig. 5 Full area Ni coating using 550 °C-29 bar nitrogen (a, b) and 400 °C-25 bar helium (c, d) as process gases, on 6061-T6 (a, c) and on Cu substrates (b, d)

critical velocity. Also, the fact that the interface of nickel-copper is smoother than that of nickel-aluminum implies that the deposition mechanisms of coatings depend on the relative deformability of the two involved materials (particle and substrate). Slightly deformed nickel particles (as shown by white arrow in Fig. 5c) can be found at the interface of nickel-aluminum.

3.3 Microstructure of Impact Interface

The interface between nickel coating and 6061-T6 substrate was shown in Fig. 6(a) by a low magnification TEM observation. The line scanning of the compositions along the interparticle (two nickel particles) boundary characterized by EDX under an STEM mode is shown in Fig. 6(b) (from point C to B). During successive impacts of nickel particles, the ''welds'' of softened aluminum formed by a high-strain rate deformation acting as a solder penetrate along the interparticle boundary to improve the bonding between the two nickel particles. The inside of the ''welds'' is free of oxygen and is mainly mixed by nickel and aluminum as depicted by Fig. 6(b). The EDX result given in Fig. 6(c) (and the table inset) confirms the fact that the oxides which may be from the native ones on the initial feedstock are concentrated into the bottom of the ''welds'' (as marked by C in Fig. 6a). As known well, the native oxide films on both substrate and particle are broken and the fresh and heated surfaces are pressed together to be bonded upon kinetic spray impact. Generally, oxides move toward the outer rim of the impact crater upon the formation of jetting through the outward movement of surface softened metals on both substrate and particle. In the present case, however slightly deformed nickel particle does not participate in jetting as mentioned above. Some chips of oxides on aluminum are pushed inside by the ''rigid'' nickel and accumulated at the bottom of the crater. Moreover, some oxides at the outer rim of the impact crater may be trapped by a subsequent impact.

The HREM images within the boxed regions B and A in Fig. 6(a) are shown in Fig. 7(a) and (b), respectively. The Fast Fourier Transformation (FFT) pattern (the inset in Fig. 7a) indicates that the ''welds'' was mainly composed of the multicrystallines of aluminum oriented along the three main crystal planes (111), (200), and (220) in terms of the three concentric rings in the inset of Fig. 7(a). As shown in Fig. 7(a)-J_1, the close view of the joint region J_1 confirms the approximately perfect bonding between nickel and aluminum. The lattices on both sides of the interface tend to arrange the atoms along some particular directions to match the two interplanar distances, e.g., between the (200) of aluminum (A) and the (111) of nickel (A_1). The same phenomenon is observed within the region J_2 with a similar interplanar distance of ~0.2 nm. Interestingly, the diffuse halo in the FFT pattern confirms the existence of amorphous aluminum within the ''welds,'' and the high indices plane with an interplanar distance of 0.41 nm at the nickel side (marked as F_2) has been confirmed according to FFT analysis.

At the tip as shown in Fig. 7(b), the ''welds'' of aluminum have an intimate contact with nickel particles at both sides. FFTs result reveals the mixture of aluminum and nickel within this region. The close view of the boxed joint region J_3 is shown in Fig. 7(b)-J_3, and FFT shows that the volume of amorphous aluminum (the diffuse halo of FFT for the inset A in Fig. 7(b)-J_3) is larger than that of F_2 in the view of J_1. Meanwhile, the transient region (box B) is mainly composed of nickel (111) and aluminum [(111)

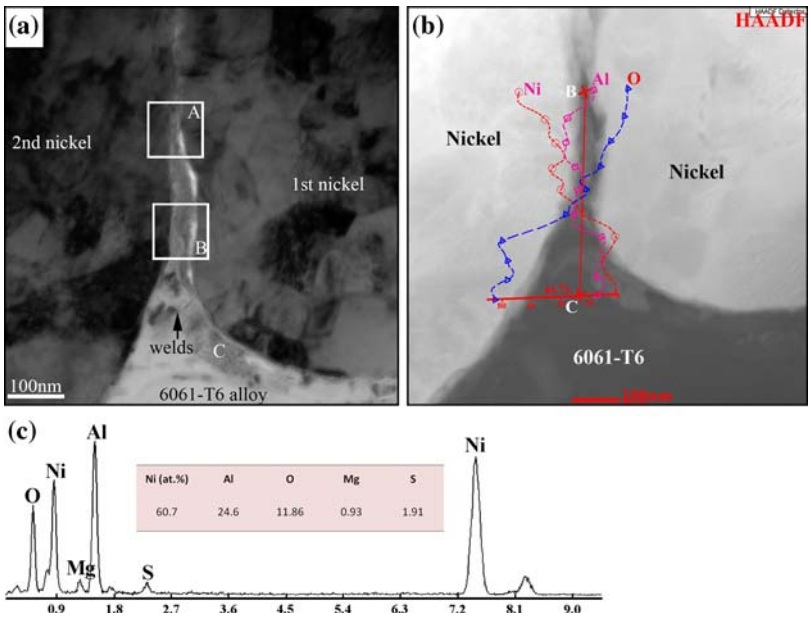

Fig. 6 TEM morphology of the ''tri-phase'' boundary between Ni coating and 6061-T6 substrate (a), the line scanning of EDX analysis along the inter-particle boundary (STEM-HAADF image) (b), and EDX result of the point C in Fig. 6a (c)

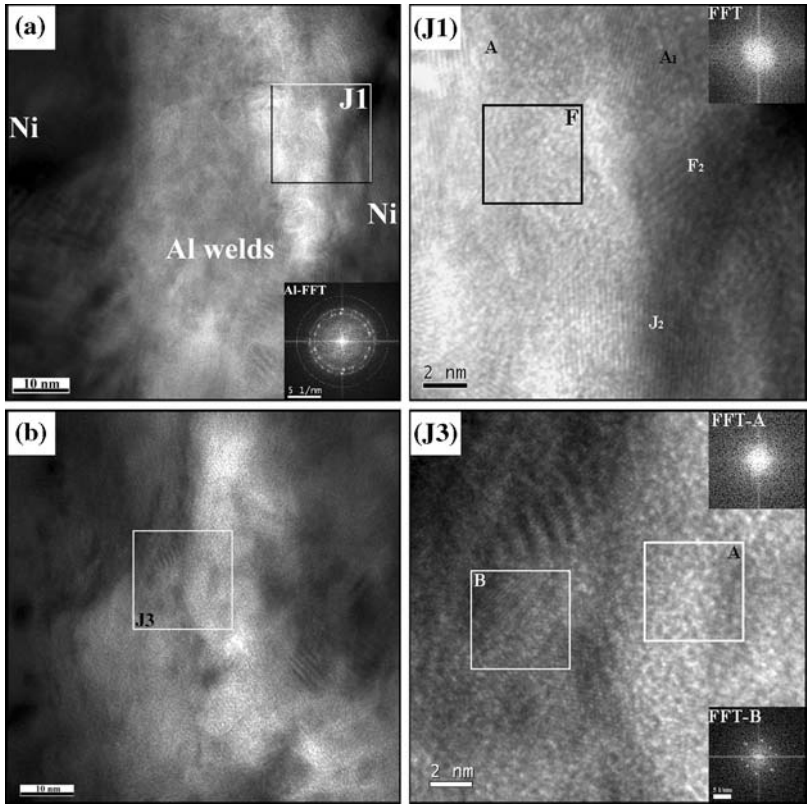

Fig. 7 Interfacial HREM images between nickel particle and metal jet taken from the boxed regions A (a) and B (b) in Fig. 6 and inset FFT patterns, polycrystalline Al consisting of (111), (200), and (220) is confirmed by diffraction rings and the transient in an atomic level from particle side (nickel) to substrate side (Al) is analyzed by FFT (J1 and J3 which taken from a and b, respectively)

and (200)] according to the FFT (inset B) analysis. Due to the overlapping of some base peaks in the diffraction patterns between elements (nickel and aluminum) and their intermetallics of nickel-aluminum, further work is needed to confirm whether the intermetallics may form within the transient region. It is worth noting that the formation of the transient region of the mixtures and the oriented arrangement of atoms at the interface may be expected to enhance the bonding between particle and substrate upon impact.

4. Discussion

In the kinetic spray process, there is a consensus that the deposition of the coatings for a certain impact system is associated with a critical velocity over which a transient from the erosion of the substrate to the deposition of the impinging particles occurs. The critical velocity is dependent on the properties of the involved materials (particles and substrate). Although critical velocity of various materials in similar cases (similar metals for particle and substrate) has been predicted using FEA (Ref 2, 23), few papers are focusing on dissimilar cases (different materials for impact counterparts) because it only takes place at the first impact (e.g., deposition onset of coatings upon impact of particle to substrate) followed by an impact of similar metals (particle to particle). Moreover, the simulation work typically considers only the case of the individual particle impact for convenience, as shown in Fig. 8. The successive impact effects through FEA (as shown in Fig. 9) and experimental examinations on the onset of coatings on the substrates have not been investigated well yet.

As shown in Fig. 8, the ASI always occurs at the side of the relatively soft materials (6061-T6 and copper in this study), as reported in our previous simulation work (Ref 21). The cross-sectional microstructures of deposits and craters (as given in Fig. 4) have a good match with the simulation results, and thus the different deposition mechanisms of nickel on these two substrates may be figured out in terms of the individual particle impact tests. As shown in Fig. 3, the deposition of individual nickel on 6061-T6 might prefer a relatively low particle velocity, but it is necessary for the nickel particle velocity over a critical velocity to successfully deposit nickel coating on copper. This results from the competition between adhesion and rebound of impinging particle in case of copper substrate upon impact.

Generally, the rebound energy which dominates the rebound of impacted particles is too low to be considered in a kinetic spray process. This is due to ASI-induced thermal softening at the impact interface resulting in a

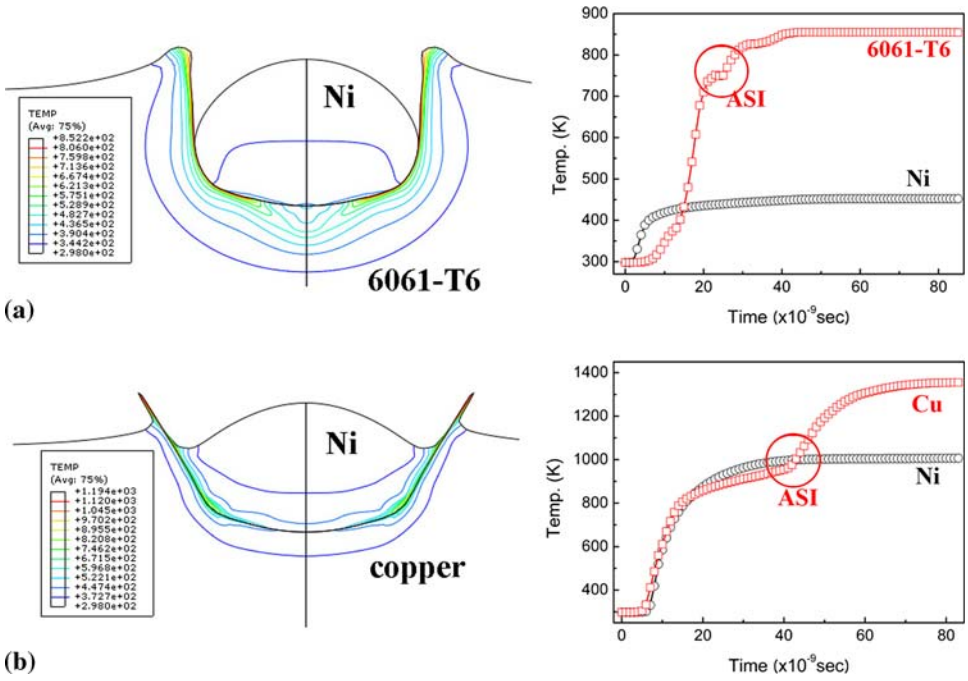

Fig. 8 Simulated temperature evolution at impact interface of Ni/6061-T6 (a) and Ni/Cu (b), and the temperature distribution at 40 ns upon an impact at 600 m/sec as simulated by ABAQUS

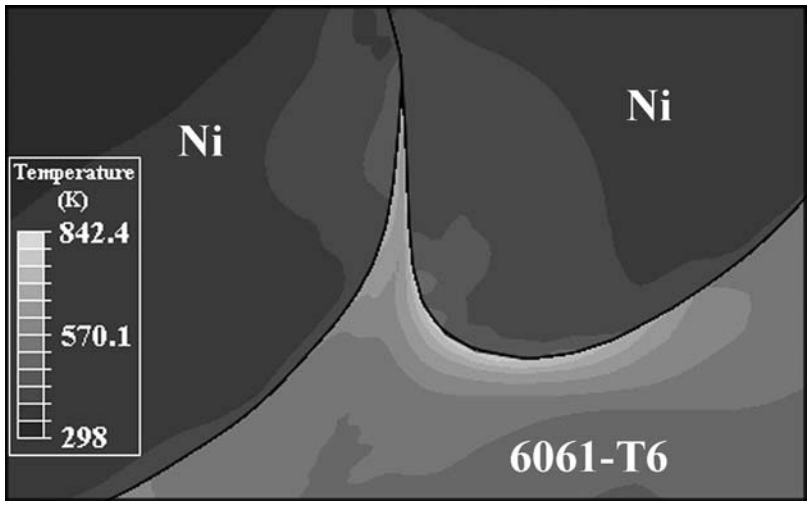

Fig. 9 The image of successive impact interface simulated using ABAQUS

considerable decrease of impact stress (approaching zero) (Ref 2). The adhesion of particle impacting on the substrate depends on the size of ASI zone. The higher the area fraction of shear strain, the stronger metallic bonding, as well as the lower recoverable strain energy can be formed. As confirmed by Gilman (Ref 24), shear strain is considered to change the symmetry of crystallographic structure in a periodic solid and is therefore more effective in stimulating reactions within those areas than in simple isotropic compression (normal strain). Such symmetry breaking destabilizes the electronic structure of bonding and makes the solid prone to chemical reactions. Hence, within the peripheral contact area at the impacted interface in case of kinetic spraying, strong metallic bonding dependent on the high fraction of shear strain is expected. Also the localized heating from the severe plastically shear deformation within this area could further increase the activity of atoms to form new metallic bonds between particle and substrate.

However, the region of ASI upon impact is relatively narrow in comparison with the whole impact interface. Out of the ASI zone, the recoverable strain energy of impact particles intuitively depends on the normal strain fraction upon impact. Accordingly, the violent rebound of

injecting particle always happens within the normal strain region (e.g., as marked by C in Fig. 4b and d).

Following the rebound theory (Ref 17), the deposition onset of particles on substrate is a competitive process between adhesion within peripheral shear strain region and rebound from central normal strain region. The rebound energy (also named as recoverable strain energy) of impacted particle in a kinetic spray process can be empirically calculated as follows (Ref 17):

$$R_e = \frac{1}{2} e_r m_p v_p^2 \quad \text{(Eq 1)}$$

$$e_r = 11.47 \left(\frac{\bar{\sigma}_Y}{E^*}\right) \left(\frac{\rho_p v_p^2}{\bar{\sigma}_Y}\right)^{-\frac{1}{4}} \quad \text{(Eq 2)}$$

Substituting Eq 2 into Eq 1, then the rebound energy R_e of particles,

$$R_e = 3.0 \left(\frac{\bar{\sigma}_Y^{\frac{5}{4}}}{E^*}\right) D^3 \rho_p^{\frac{3}{4}} v_p^{\frac{3}{2}}, \quad \text{(Eq 3)}$$

where D, ρ_p, m_p, and v_p are, respectively, the diameter, density, molecular weight, and velocity of impinging particle. e_r is the recoil coefficient. $\bar{\sigma}_Y$ is the effective yield stress during impact, and E^* is the conventional elastic modulus of particle and substrate. Obviously, elastic modulus is inversely proportional to rebound energy of the particle. Thus, the rebound energy of Ni particles on 6061-T6 Al alloy substrate is higher than that on Cu substrate due to a lower elastic modulus of this Al alloy as given in Table 1. Meanwhile, particle velocity and effective yield stress at impact interface are competitive to affect rebound energy. That is, rebound energy increases with particle velocity, accompanying with decreasing effective yield stress $\bar{\sigma}_Y$, and the adhesion energy also increase with increasing thermal softening area at impact interface due to the increasing kinetic energy of impinging particle.

According to the simulation results as given in Fig. 8, the interface temperature exhibits a substantial difference between the two impact cases (Ni to Al and Ni to Cu). Depending on the deformation degree upon impact, the temperature evolutions on both sides of impact couples (particle and substrate) are different. ASI always occurs only at the side of the relatively softer substrates (e.g., 6061-T6 and Cu) in terms of an abnormal increase of interface temperature, but the temperature at the relatively harder nickel particle side shows a stable increase upon impact. Also, the interface temperature approaches melting points of the substrates (both 6061-T6 and Cu) with an impinging particle velocity of 600 m/s which is greater than the estimated critical velocity of nickel according to Ref 23. The nickel particle temperature is dependent on its deformation degree in the two impact cases. More severe plastic deformation of Ni particle on Cu substrate leads to a higher particle temperature than that on 6061-T6 substrate. Thus, higher interface temperature and more serious shear deformation of Ni particle on Cu substrate induce a wider thermal softening zone than Ni-Al impact case. In addition, the difference in deformability between particle and substrate dominates the dissipation of kinetic energy of injecting particles. Due to the substantial difference in deformability between Ni and Al, high rebound energy is retained after the sole dissipation of kinetic energy to the deformation of 6061-T6 substrate. However, the kinetic energy is mainly dissipated to the comparable deformation between Ni particle and Cu substrate in the other impact case. The ABAQUS calculations also confirm much higher rebound energy of Ni particle from 6061-T6 substrate (1411.9×10^{-9} J) than that from Cu substrate (640.9×10^{-9} J). Hence, the BR of Ni powder on 6061-T6 substrate is much less than that on Cu substrate in the case of individual impact at the same parameters. It is worth noting that rebound and weak adhesion at the central interface between Ni deposit and Cu substrate upon impact are confirmed in terms of a seam formation (marked by C in Fig. 3d). The phenomenon has also been reported in terms of a TEM observation (Ref 18).

According to the cross-sectional morphologies of deposits and craters as shown in Fig. 4, the deposition of Ni particle on 6061-T6 substrate mainly depends on the embedding, but the adhesion between Ni deposits and Cu substrate through a simultaneous and comparable deformation of the involved materials dominates the deposition onset of coatings. A particle velocity above the critical velocity is needed to get nickel deposits on copper substrate. As mentioned above, the rebound energy of Ni particle on 6061-T6 substrate increases with particle velocity according to Eq 3, and thus the BR decreases.

In contrast, the increasing contact area with particle velocity leads to the increase of adhesion strength between Ni deposit and Cu, and an increase of resultant BR (as shown in Fig. 4). One can find there is a peak of particle velocity of 762 m/s (calculated by equation in Ref 22) after which the BR of nickel powder on Cu decreases with further increasing particle velocity. That is in a good agreement with the rebound theory of kinetic spray impacts in Ref 17. Obviously, it seems that the increase of bound force is faster than the adhesion strength of nickel on Cu with increasing impinging particle velocity, and thus the rebound exceeds the adhesion strength as the peak velocity reaches and is exceeded.

Other than the individual particle impact case, the deposition onset of full nickel coating on both substrates would be inevitably influenced by many factors, such as embedding, mechanical interlocking, and tamping of successive impacts. However, the influence of those factors is quite different case by case. In the impact case of a harder particle to a softer substrate (i.e., Ni to relatively soft 6061-T6 substrate), the effects of successive impacts and cold welds of viscous metal on bonding of impinging particles play dominant roles in triggering full coating (as shown in Fig. 9 of simulated results). In impact case of involved materials with comparable deformability (i.e., Ni particle to Cu substrate), the deposition onset of coating is mainly dependent on the formation of metallurgical bonds resulting from the synchronous shear deformation of substrate and particle and the occurrence of ASI upon impact. Hence, although the occurrence of ASI at impact

interface is always considered to characterize the deposition of kinetic sprayed coatings (e.g. Ni to Cu), it seems not to be the only criteria for critical velocity to evaluate the deposition onset of kinetic spray coatings on a relatively softer substrate (e.g. Ni on soft 6061-T6 substrate).

Within a relatively wide particle velocity distribution, full Ni coating could be successfully started on 6061-T6 substrate, i.e., the coating can even be triggered at a low parameter of 300 °C-15 bar nitrogen process gas [the calculated impact velocity (Ref 22) of 443 m/s]. The embedding and cold welds of high temperature metals (such as Al in this study) play important roles in the deposition onset of the thin nickel coating on 6061-T6 through controlling the rebound of impinging particles (as shown in Fig. 5a). Then, it is possible for using an irregular powder to increase the mechanical interlock and embedding of impacted particles and to easily trigger kinetic spray coatings on a relatively soft substrate. As seen in Fig. 6, the rebound of previous impact particle might be hindered by successive impact. Meanwhile, the high temperature viscous Al as a solder is extruded into the inter-particle boundary to improve the adhesion strength of the successive particle. Although simulated interface temperature is lower than melting point of Al, the melting might occur at the impact interface due to the decrease of melting point under a nonequilibrim strain. Monte Carlo simulations suggested that FCC elemental crystals under uniaxial tension can undergo stress-induced melting at temperatures $T_m(\sigma)$ well below the thermodynamic melting temperature $T_m(\sigma = 0)$ of the corresponding unstressed crystal (Ref 25). Consequently, the rapid solidification [cooling rate can reach up to 10^{10} K/s in kinetic spray process (Ref 2)] of the thin melted Al layer captures the injecting particles and enhances bond strength between coating and substrate. It is worth noting that the ''cold weld'' effect of high temperature viscous metal on the deposition onset of kinetic spray coatings, regardless of melting, might take place in almost all impact cases. However, the growth of coatings on the previously triggered layer needs a particle velocity high enough (typically over the critical velocity) to achieve strong metallurgical bonding between the two impacted particles (similar metal). In addition, it needs further research on atomic realignment upon impact at a high-strain rate to describe detailed bonding process of kinetic spray coatings and to confirm whether intermetallic compounds form within an extremely short impact time at the impact interface.

5. Conclusions

In a kinetic spray process, the dissipation of kinetic energy of impinging particles is dominated by the relative deformability of impact couples. The results indicates that the deposition onset of nickel coating on two substrates (6061-T6 and Cu) shows different deposition mechanisms related to the nature of substrate. On 6061-T6, the BR of nickel is lower than that on Cu in the case of individual particle impact, but the DE on both substrates is comparable in the case of full coating deposition using helium process gas. That is, embedding, tamping and ''cold weld'' of viscous metal at the impact interface play dominant roles in the coating deposition onset on the relatively softer 6061-T6 substrate. Thus, the coating can be triggered on the relatively softer substrate with a low particle velocity in order to avoid the violent rebound. A critical velocity must be exceeded in case of the impact of materials with comparable deformability (e.g., nickel to copper) to trigger a kinetic spray coating which is dependent on forming metallurgical adhesion at the peripheral impact interface.

Acknowledgments

This work was supported by the Korea Science and Engineering Foundation (KOSEF) grant funded by the Korea Government (MOST) (No. 2006-02289), Natural Science Foundation of China (NSFC) (Grant Nos. 50904081 & 50721003), and the joint program NSFC-KOSEF (Grant No. 50911140283).

References

1. A.P. Alkhimov, V.F. Kosarev, N.I. Nesterovich, and A.N. Papyrin, Method of Applying Coatings, Russian Patent 1,618,778, 8 Sep 1990, priority of the invention 6 June 1986
2. H. Assdi, F. Gärtner, T. Stoltenhoff, and H. Kreye, Bonding Mechanism in Cold Gas Spraying, *Acta Mater.*, 2003, **51**, p 4379-4394
3. W. Choi, L. Li, V. Luzin, R. Neiser, T. Gnäupel-Herold, H. Prask, S. Sampath, and A. Gouldstone, Integrated Characterization of Cold Sprayed Aluminum Coatings, *Acta Mater.*, 2007, **55**, p 857-866
4. T. Marrocco, D. McCartney, P. Shipway, and A. Sturgeon, Production of Titanium Deposits by Cold-Gas Dynamic Spray: Numerical Modeling and Experimental Characterization, *J. Therm. Spray Technol.*, 2006, **15**, p 263-272
5. W. Li, X. Guo, C. Verdy, L. Dembinski, H. Liao, and C. Coddet, Improvement of Microstructure and Property of Cold-Sprayed Cu-4 at%Cr-2 at%Nb Alloy by Heat Treatment, *Scripta Mater.*, 2006, **55**, p 327-330
6. Q. Zhang, C. Li, C. Li, G. Yang, and S. Lui, Study of Oxidation Behavior of Nanostructured NiCrAlY Bond Coatings Deposited by Cold Spraying, *Surf. Coat. Technol.*, 2008, **202**, p 3378-3384
7. P. Sudharshan Phani, V. Vishnukanthan, and G. Sundararajan, Effect of Heat Treatment on Properties of Cold Sprayed Nanocrystalline Copper Alumina Coatings, *Acta Mater.*, 2007, **55**, p 4741-4751
8. H. Wang, C. Li, G. Yang, C. Li, Q. Zhang, and W. Li, Microstructural Characterization of Cold-Sprayed Nanostructured FeAl Intermetallic Compound Coating and Its Ball-Milled Feedstock Powders, *J. Therm. Spray Technol.*, 2007, **16**, p 669-676
9. H. Na, G. Bae, S. Shin, S. Kumar, H. Kim, and C. Lee, Advanced Deposition Characteristics of Kinetic Sprayed Bronze/Diamond Composite by Tailoring Feedstock Properties, *Comp. Sci. Technol.*, 2009, **69**, p 463-468
10. Y. Xiong, K. Kang, S. Yoon, and C. Lee, The Fabrication of Carbon Nanotubes Reinforced Copper Coating by a Kinetic Spray Process, *J. Nanosci. Nanotechnol.*, 2008, **8**, p 5561-5565
11. S. Yoon, Y. Xiong, H. Kim, and C. Lee, Dependence of Initial Powder Temperature on Impact Behavior of Bulk Metallic Glasses in a Kinetic Spray Process, *J. Phys. D Appl. Phys.*, 2009, **42**, p 082004-082008
12. H. Lee, Y. Yu, Y. Lee, Y. Hong, and K. Ko, Thin Film Coatings of WO_3 by Cold Gas Dynamic Spray: A Technical Note, *J. Therm. Spray Technol.*, 2005, **14**, p 183-186

13. H. Kim, C. Lee, and S. Hwang, Fabrication of WC-Co Coatings by Cold Spray Deposition, *Surf. Coat. Technol.*, 2005, **191**, p 335-340
14. C. Li, G. Yang, P. Gao, J. Ma, Y. Wang, and C. Li, Characterization of Nanostructured WC-Co Deposited by Cold Spraying, *J. Therm. Spray Technol.*, 2007, **16**, p 1011-1020
15. M. Yandouzi, E. Sansoucy, L. Ajdelsztajn, and B. Jodoin, WC-Based Cermet Coatings Produced by Cold Gas Dynamic and Pulsed Gas Dynamic Spraying Processes, *Surf. Coat. Technol.*, 2007, **202**, p 382-390
16. R. Dykhuizen, M. Smith, D. Gilmore, R. Neiser, X. Jiang, and S. Sampath, Impact of High Velocity Cold Spray Particles, *J. Therm. Spray Technol.*, 1999, **8**, p 559-564
17. J. Wu, H. Fang, S. Yoon, H. Kim, and C. Lee, The Rebound Phenomenon in Kinetic Spraying Deposition, *Scripta Mater.*, 2006, **54**, p 665-669
18. K. Kim, M. Watanabe, K. Mitsuishi, K. Iakoubovskii, and S. Kuroda, Impact Bonding and Rebounding Between Kinetically Sprayed Titanium Particle and Steel Substrate Revealed by High-Resolution Electron Microscopy, *J. Phys. D Appl. Phys.*, 2009, **42**, p 065304-065308
19. Mata web (Material Property Data). Available from: www.matweb.com (Automation Creations, Inc), and Davis, J.R., Ed., *ASM Handbook: Volume 2, Properties and Selection: Nonferrous Alloys and Special-Purpose Material*, ASM International (Materials Park, OH), 1990, p 405, 760 and 1840
20. *ABAQUS 6.7-2 User Manual*, Hibbit, Karlsson & Soerensen Inc. (Pawtucket, RI), 2007
21. G. Bae, Y. Xiong, S. Kumar, K. Kang, and C. Lee, General Aspects of Interface Bonding in Kinetic Sprayed Coatings, *Acta Mater.*, 2008, **56**, p 4858-4868
22. J. Wu, H. Fang, S. Yoon, H. Kim, and C. Lee, Measurement of Particle Velocity and Characterization of Deposition in Aluminum Alloy Kinetic Spraying Process, *Appl. Surf. Sci.*, 2005, **252**, p 1368-1377
23. T. Schmidt, F. Gärtner, H. Assadi, and H. Kreye, Development of a Generalized Parameter Window for Cold Spray Deposition, *Acta Mater.*, 2006, **54**, p 729-742
24. J.J. Gilman, Mechanochemistry, *Science*, 1996, **274**, p 65
25. R.M. Lynden-Bell, A Simulation Study of Induced Disorder, Failure and Fracture of Perfect Metal Crystals Under Uniaxial Tension, *J. Phys.: Condens. Matter.*, 1995, **7**, p 4603-4624